01

High-frequency conductivity of a metal nanolayer taking into account the size quantization effects and conductor band structure anisotropy

© O.M. Savenko, I.A. Kuznetsova

Demidov State University,
Yaroslavl, Russia
e-mail: savenko.oleg92@mail.ru

Received July 28, 2025
Revised October 3, 2025
Accepted October 21, 2025

A theoretical task solution of metallic nanolayer high-frequency electrical conductivity is obtained, taking into account the electron quantum confinement effects. The conductor Fermi surface is an ellipsoid of revolution with its principal axis oriented parallel to the nanolayer plane. It is assumed that the electric field frequency does not exceed the plasma resonance frequency. Analytical expressions are derived for the conductivity tensor components, depending on the dimensionless parameters: nanolayer thickness, electric field frequency, nanolayer boundary roughness parameters and Fermi surface ellipticity parameter. A comparative analysis of the obtained results with known experimental data for a bismuth film is performed.

Keywords: nanolayer, conductivity, Liouville equation, Soffer model, Fermi surface.

DOI: 10.61011/TP.2026.03.63152.161-25

Introduction

Conducting nanolayers are used widely in various fields of nanoelectronics, optoelectronics, microwave electronics, and solar power engineering [1–5]. This is attributable to the active development of technologies of fabrication of nanolayers with a thickness of several nanometers [6]. The current trend is toward the reduction in characteristic dimensions of integrated circuits; the degree of integration has reached billions of transistors per square millimeter. Multilayer nanocoatings have provided an opportunity to increase significantly the energy efficiency of solar cells. Rational use of layered nanostructures necessitates the development and improvement of theoretical models that characterize their parameters (electrical, optical, etc.). The quantization of the energy spectrum of carriers needs to be taken into account in nanolayers with a thickness on the order of nanometers. The behavior of carriers is influenced to a significant extent by surface roughness at the atomic level. Theoretical models incorporating the effects of quantum confinement and surface scattering of carriers are needed in order to characterize properly the electrical parameters of nanolayers.

The contribution of surface scattering of conduction electrons to the electrical and galvanomagnetic characteristics of thin films has been studied in sufficient detail. Different models of surface scattering of carriers (Fuchs and Soffer boundary conditions) were used in [7–13]. Note that the quasi-classical approximation was used in [7–13].

The first studies where the quantization of the energy spectrum of carriers and the surface roughness were taken into account have been published at the end of the 20th century [14–17]. The Green's function method, which stipulates that the wave functions in a quantum well be determined by solving the Dyson equation, was used in [14,15]. Other research groups [16,17] performed a direct calculation of the Hamiltonian established by carrier scattering. The authors of the above-mentioned studies limited themselves to the case of a metal and a constant electric field.

In a relatively recent paper [18], the problem of static electrical conductivity of a conducting nanolayer was solved using the method that takes into account the surface scattering of carriers through the Soffer boundary conditions [19]. A nanolayer of metal and semiconductor materials was considered in [18]. In the former case, the dependence of the Fermi energy on nanolayer thickness was taken into account (it was assumed that the Fermi level is determined by the upper filled energy level). In the latter case, the dependence of the density of free carriers on thickness was assumed. A theoretical model of electrical conductivity of a semiconductor nanolayer in an alternating electric field was constructed in [20]. The case of a metal nanolayer was not considered.

Note that the problems posed in [18,20] were solved with account for the ellipsoidal band structure of the conductor, which is attributable to the following. The constant energy surface of silicon and germanium semiconductors, which are used often in micro- and nanoelectronics, contains several ellipsoids of revolution. Quantum confinement effects are weak in typical metals with a spherical Fermi surface, since the de Broglie wavelength of conduction electrons is close to 0.3 nm (is on the order of the interatomic distance) [21]. Quantum effects are well-pronounced in semi-metal bismuth and its alloys with antimony [22] (the de Broglie wavelength here is on the order of 30 nm [23]). The Fermi surface of electrons in bismuth is represented by three symmetrically positioned ellipsoids of revolution.

In the present study, a solution to the problem of electrical conductivity of a metal nanolayer in an alternating electric field is obtained with account for the ellipsoidal shape of the Fermi surface and the Soffer boundary conditions model.

1. Problem formulation

Let us consider a metal or semi-metal nanolayer of thickness a. Electric field $\mathbf{E}$ is applied parallel to the plane of the nanolayer (Fig. 1, a) and varies with time as

$$\mathbf{E} = \mathbf{E}_0 \exp(-i\omega t), \tag{1}$$

where ω is the electric field frequency.

The relation between the nanolayer thickness and the de Broglie wavelength of carriers may be arbitrary. The effects of quantum confinement of conduction electrons in the direction perpendicular to the layer surface need to be taken into account in this case. The energy spectrum in the direction of the Z axis will consist of several subbands (Fig. 1, b). Electron gas in the nanolayer may be treated as a quasi-two-dimensional gas in a quantum well. It is assumed that the metal nanolayer borders on dielectric layers only. Nanostructures containing metal–semiconductor junctions are not considered. The height of walls of the potential well will be greater than 1.5 eV (this follows from the fact that a 3 eV width of the forbidden band is the conditional boundary between semiconductor and dielectric materials). This condition is sufficient to consider the wall height of the potential well to be infinite. It is assumed that the constant energy surface has the form of an ellipsoid of revolution with its principal axis oriented parallel to the plane of the nanolayer (Fig. 1, b). Let us examine the scenario where the rotation axis of the Fermi ellipsoid is oriented parallel to the X axis. The total energy of an electron (hole) in the lth subband is expressed as follows:

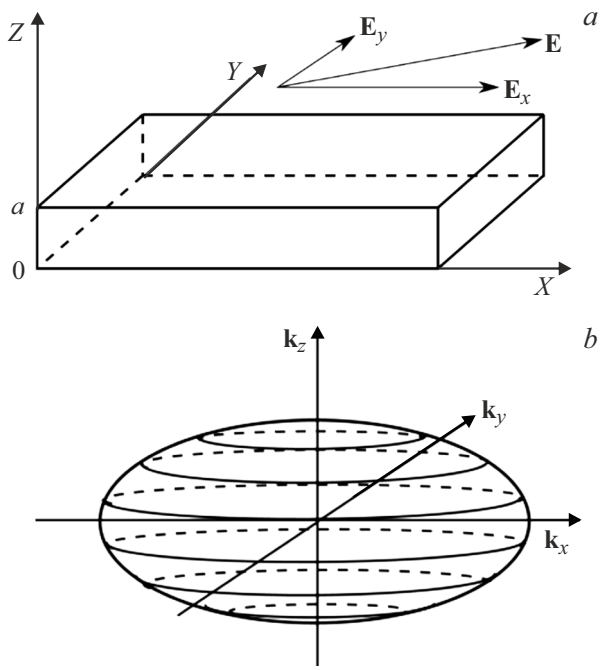

Figure 1. a — Thin metal nanolayer in a longitudinal electric field; b — shape of the constant energy surface of the conductor.

$$\varepsilon_l = \frac{p_x^2}{2m_{\|}} + \frac{p_y^2}{2m_{\perp}} + \varepsilon_1 l^2, \;\; l = \pm 1, \pm 2, \pm 3, \ldots, \pm N, \tag{2}$$

where $m_{\|}$ and $m_{\perp}$ are the longitudinal and transverse effective masses of a charge carrier, respectively; $\varepsilon_1 = (\pi\hbar)^2/(2m_{\perp}a^2)$ is the eigenvalue of the electron energy in the first subband; and N is the total number of subbands.

In the present study, electron-electron scattering, which becomes significant only at sufficiently low temperatures and in pure samples, is neglected. It has been established that the main contribution to the processes of carrier transport in bismuth at temperatures above 77 K is made by scattering off thermal vibrations of the crystal lattice [24]. Let us consider the upper limit of temperatures at which the theoretical model is valid. The degeneracy temperature in typical metals is on the order of 10^4 K. Electron gas may be considered degenerate up to the melting point of a metal. Owing to the low carrier density (on the order of $10^{17}\,\mathrm{cm}^{-3}$), the temperature of transition of electron gas to a non-degenerate state in bismuth semi-metals is relatively low (around 100 K) [25]. However, studies demonstrate that the band structure and carrier density may change in bismuth films deposited on dielectric substrates. This is attributable to the presence of microdeformations in bismuth films. For example, the density in pure bismuth films deposited on a mica substrate may reach $2 \cdot 10^{18}\,\mathrm{cm}^{-3}$ [26]. In this case, the degeneracy temperature will be close to 400 K; i.e., the theoretical model of the present study may be applied to bismuth films at room temperatures.

According to quantum theory, the carrier system is characterized by the density operator [27]:

$$\hat{\rho}(t) = \sum_l W_l |\psi_l(t)\rangle\langle\psi_l(t)|, \tag{3}$$

which obeys the Liouville equation

$$i\hbar \frac{\partial \hat{\rho}(t)}{\partial t} = [\hat{H}(t), \hat{\rho}(t)]. \tag{4}$$

Here, $\psi_l(t)$ is the electron wave function, $\hat{H}(t)$ is the Hamiltonian of the system, and W_l is a coefficient characterizing the probability that the carrier system is in state ψ_l.

A slight deviation of the carrier system from the equilibrium state is allowed. The density operator may be written as the sum of equilibrium operator $\hat{\rho}^{(0)}$ and small non-equilibrium correction $\hat{\rho}^{(1)}$:

$$\hat{\rho}(\mathbf{k}_{\|}, z, t) = \hat{\rho}^{(0)}(\varepsilon_l) + \hat{\rho}^{(1)}(\mathbf{k}_{\|}, z) \exp(-i\omega t), \tag{5}$$

where $\mathbf{k}_{\|}$ is the wave vector component parallel to the plane of the nanolayer.

Under condition (5) (see Appendix), Eq. (4) may be reduced to a kinetic equation in the relaxation time τ approximation:

$$-i\omega\left(f_{l\|}^{(1)}+f_{l\perp}^{(1)}\right)+\frac{\hbar k_{zl}}{m_\perp}\frac{\partial\left(f_{l\|}^{(1)}+f_{l\perp}^{(1)}\right)}{\partial z}+\frac{e\mathbf{E}}{\hbar}\frac{\partial f_l^{(0)}}{\partial \mathbf{k}_\|}+\frac{f_{l\|}^{(1)}}{\tau_\|}+\frac{f_{l\perp}^{(1)}}{\tau_\perp}=0. \quad (6)$$

Here, $\tau_\|$ and $\tau_\perp$ are the longitudinal and transverse components of the relaxation time tensor, respectively; e is the electron charge; $\hbar$ is the Planck constant; and k_{zl} is the z component of the wave vector of a carrier in the lth subband. Note that carrier distribution function f_l plays the part of diagonal elements of the density matrix in Eq. (6), which may be presented in a linear approximation with respect to the external field:

$$f_l(\mathbf{k}_\|,z,t)=f_l^{(0)}(\varepsilon_l)+f_l^{(1)}(\mathbf{k}_\|,z)\exp(-i\omega t), \quad (7)$$

$$f_l^{(1)}(\mathbf{k}_\|,z)=f_{l\|}^{(1)}(\mathbf{k}_\|,z)+f_{l\perp}^{(1)}(\mathbf{k}_\|,z),$$

$$f_l^{(0)}(\varepsilon_l)=\begin{cases}1, & 0<\varepsilon_l<\varepsilon_\mathrm{F},\\ 0, & \varepsilon_l>\varepsilon_\mathrm{F},\end{cases}$$

where $f_l^{(0)}$ is the equilibrium distribution function; $f_{l\|}^{(1)}$ and $f_{l\perp}^{(1)}$ are non-equilibrium corrections characterizing the deviation of the distribution function from the equilibrium one in directions parallel to the principal and secondary axes of the constant energy ellipsoid, respectively; and ε_F is the Fermi energy.

The surface scattering of carriers is taken into account using the Soffer boundary conditions [19] imposed on Eq. (6):

$$\begin{cases} f_{l\|,\perp}^{(1)+}=q_1(g_1,\theta)f_{l\|,\perp}^{(1)-} & \text{for } z=0,\\ f_{l\|,\perp}^{(1)-}=q_2(g_2,\theta)f_{l\|,\perp}^{(1)+} & \text{for } z=a,\end{cases} \quad (8)$$

$$q_{1,2}(g_{1,2},\theta)=\exp\left(-(4\pi g_{1,2}\cos\theta)^2\right),$$

$$g_{1,2}=g_{s1,2}/\lambda_\mathrm{F}.$$

Here, $f_{l\|}^{(1)+}$ and $f_{l\perp}^{(1)+}$ are non-equilibrium corrections to the electron distribution function with $k_{zl}>0$; $f_{l\|}^{(1)-}$ and $f_{l\perp}^{(1)-}$ are non-equilibrium corrections with $k_{zl}<0$; λ_F is the de Broglie wavelength of an electron with the Fermi energy; g_{s1} and g_{s2} are the root-mean-square heights of surface relief of the lower and upper boundaries of the nanolayer, respectively; and θ is the angle between the direction of the electron wave vector and the normal to the nanolayer surface.

2. Mathematical calculations

Solving Eq. (6) with boundary condition (8) taken into account, we obtain expressions for non-equilibrium corrections to the carrier distribution function

$$f_{l\|}^{(1)+}(z)=-\frac{e(v_x\cdot E_x)}{\nu_\|}\frac{\partial f_l^{(0)}}{\partial\varepsilon_\|}\left(1-\phi_{l\|}^{+}e^{-\Omega_{l\|}\xi}\right), \quad (9)$$

$$f_{l\perp}^{(1)+}(z)=-\frac{e(v_y\cdot E_y)}{\nu_\perp}\frac{\partial f_l^{(0)}}{\partial\varepsilon_\|}\left(1-\phi_{l\perp}^{+}e^{-\Omega_{l\perp}\xi}\right), \quad (10)$$

$$f_{l\|}^{(1)-}(z)=-\frac{e(v_x\cdot E_x)}{\nu_\|}\frac{\partial f_l^{(0)}}{\partial\varepsilon_\|}\left(1-\phi_{l\|}^{-}e^{\Omega_{l\|}(1-\xi)}\right), \quad (11)$$

$$f_{l\perp}^{(1)-}(z)=-\frac{e(v_y\cdot E_y)}{\nu_\perp}\frac{\partial f_l^{(0)}}{\partial\varepsilon_\|}\left(1-\phi_{l\perp}^{-}e^{\Omega_{l\perp}(1-\xi)}\right). \quad (12)$$

The following notation was introduced:

$$\phi_{l\|,\perp}^{+}=\frac{(1-q_1)+q_1(1-q_2)e^{-\Omega_{l\|,\perp}}}{1-q_1q_2e^{-2\Omega_{l\|,\perp}}},$$

$$\phi_{l\|,\perp}^{-}=\frac{(1-q_2)+q_2(1-q_1)e^{\Omega_{l\|,\perp}}}{1-q_1q_2e^{2\Omega_{l\|,\perp}}},$$

$$\Omega_{l\|,\perp}=a\nu_{\|,\perp}/(v_1 l);\quad \xi=z/a.$$

Here, $\nu_{\|,\perp}=\tau_{\|,\perp}^{-1}-i\omega$ are the complex frequencies of carrier scattering in directions parallel to the principal and secondary axes of the ellipsoid of constant energy, respectively, and $\varepsilon_\|$ is the longitudinal kinetic energy of an electron.

The current density is written as [18]

$$\mathbf{j}=\frac{2ek_1}{(2\pi)^3}\sum_l\int\int\mathbf{v}\left(f_l^{(1)+}+f_l^{(1)-}\right)dk_xdk_y. \quad (13)$$

Let us rewrite expression (13) for the components of current density on axes X and Y:

$$j_x=\frac{2ek_1}{(2\pi)^3}\sum_l\int\int v_x\left(f_{l\|}^{(1)+}+f_{l\|}^{(1)-}\right)dk_xdk_y, \quad (14)$$

$$j_y=\frac{2ek_1}{(2\pi)^3}\sum_l\int\int v_y\left(f_{l\perp}^{(1)+}+f_{l\perp}^{(1)-}\right)dk_xdk_y. \quad (15)$$

Integrals (14) and (15) are easier to calculate in coordinate system $(\varepsilon_\|,\varphi)$. The relation between coordinates (k_x,k_y) and $(\varepsilon_\|,\varphi)$ is given by the following system of equations:

$$\begin{cases} k_x=\dfrac{\sqrt{2m_\|\varepsilon_\|}}{\hbar}\cos\varphi,\\ k_y=\dfrac{\sqrt{2m_\perp\varepsilon_\|}}{\hbar}\sin\varphi.\end{cases} \quad (16)$$

Inserting (9)–(12), (16) into (14) and (15) and performing the necessary calculations, we obtain the following expressions for the x and y components of current density:

$$j_x = \frac{4\pi e^2 m_0^{3/2} E_x \sqrt{2\varepsilon_1}}{\nu_\parallel h^3 m_\parallel} \sum_{l=1}^{N} (\varepsilon_F - \varepsilon_1 l^2) \times (2 + \phi_{l\parallel}^{+} e^{-\Omega_{l\parallel}\xi} + \phi_{l\parallel}^{-} e^{-\Omega_{l\parallel}(1-\xi)}), \quad (17)$$

$$j_y = \frac{4\pi e^2 m_0^{3/2} E_x \sqrt{2\varepsilon_1}}{\nu_\perp h^3 m_\perp} \sum_{l=1}^{N} (\varepsilon_F - \varepsilon_1 l^2) \times (2 + \phi_{l\perp}^{+} e^{-\Omega_{l\perp}\xi} + \phi_{l\perp}^{-} e^{-\Omega_{l\perp}(1-\xi)}), \quad (18)$$

where the scalar effective electron mass is denoted as $m_0 = \sqrt[3]{m_\parallel m_\perp^2}$.

We assume that the carrier density in a metal does not change. According to the band theory, the Fermi energy in a metal is determined by the upper filled energy level. As the layer becomes thinner, the number of allowed energy states decreases. If the carrier density is considered to be a constant value, the Fermi level should change with a change in thickness. Similar reasoning was presented in [28] for thin films of aluminum and gold. It was demonstrated that the Fermi energy increases with decreasing thickness and the dependence of the Fermi energy on thickness is oscillatory in nature. Let us use the dependence of the Fermi energy on nanolayer thickness obtained in [18]:

$$\rho^2 = \frac{2}{3N}\rho_v^3 + \frac{1}{6}(N+1)(2N+1), \quad (19)$$

$$\rho = \sqrt{\varepsilon_F/\varepsilon_1}, \quad \rho_v = \sqrt{\varepsilon_{Fv}/\varepsilon_1},$$

where ε_{Fv} is the Fermi energy without account for the quantization of the energy spectrum of carriers (macroscopic sample) and N is the total number of filled subbands, which is given by

$$N = \mathrm{int}\left[\sqrt[3]{\frac{p}{2} + \sqrt{Q}} + \sqrt[3]{\frac{p}{2} - \sqrt{Q}} + \frac{1}{4}\right], \quad (20)$$

$$Q = \left(\frac{p}{2}\right)^2 - \left(\frac{7}{48}\right)^3, \quad p = \frac{3}{32} + \rho_v^3.$$

The components of the integral conductivity tensor are determined using formulae (21)–(23). When the principal axis of the Fermi ellipsoid is oriented parallel to the X axis, the conductivity is a second-rank diagonal tensor:

$$G = \begin{pmatrix} G_\parallel & 0 \\ 0 & G_\perp \end{pmatrix}, \quad (21)$$

$$G_\parallel = \int_0^a \sigma_\parallel dz = a \int_0^1 \frac{j_x}{E_x} d\xi, \quad (22)$$

$$G_\perp = \int_0^a \sigma_\perp dz = a \int_0^1 \frac{j_y}{E_y} d\xi. \quad (23)$$

Inserting (17) and (18) into (22) and (23), we obtain expressions for the longitudinal and perpendicular components of the conductivity tensor:

$$G_{\parallel,\perp} = \sigma_0 a \Sigma_{\parallel,\perp}(x_0, x_\lambda, y_0, \gamma, g_1, g_2), \quad (24)$$

$$\Sigma_\parallel = \frac{\gamma^2}{z_{0\parallel}}\left\{1 - \frac{3}{16 x_0^3 \gamma^{1.5}} \sum_{l=1}^{N} (\rho^2 - l^2)\chi\left(\frac{2x_0^2 z_{0\parallel}\gamma}{l x_\lambda}\right)\right\}, \quad (25)$$

$$\Sigma_\perp = \frac{1}{\gamma z_{0\perp}}\left\{1 - \frac{3}{16 x_0^3 \gamma^{1.5}} \sum_{l=1}^{N} (\rho^2 - l^2)\chi\left(\frac{2x_0^2 z_{0\perp}\gamma}{l x_\lambda}\right)\right\}. \quad (26)$$

The following parameters were introduced:

$$\sigma_0 = \frac{n e^2 \tau_{0v}}{m_0}, \quad \tau_{0v} = \sqrt[3]{\tau_{v\parallel}\tau_{v\perp}^2},$$

$$\chi(p) = \frac{1}{2p}(1 - e^{-p})\frac{2 - q_1 - q_2 + (q_1 + q_2 - 2q_1 q_2)e^{-p}}{1 - q_1 q_2 e^{-2p}},$$

$$q_{1,2}(g_{1,2}, \theta) = \exp\left(-(2\pi g_{1,2} l/x_0)^2\right),$$

$$z_{0\parallel} = \frac{\rho\sqrt{\gamma}}{2x_0} - i y_0, \quad z_{0\perp} = \frac{\rho}{2x_0\gamma} - i y_0, \quad \gamma = \frac{m_\perp}{m_0},$$

$$\rho^2 = \frac{16}{3N} x_0^3 \gamma^{1.5} + \frac{1}{6}(N+1)(2N+1),$$

$$x_0 = \frac{a}{\lambda_{F0}}, \quad x_\lambda = \frac{\Lambda}{\lambda_{F0}}, \quad y_0 = \omega\tau_{0v}.$$

Here, σ_0 is the classical conductivity without quantum confinement effects; τ_{0v} is the scalar relaxation time in a macroscopic sample; and $\Sigma_\parallel$ and $\Sigma_\perp$ are the dimensionless longitudinal and transverse components of the conductivity tensor, which are functions of dimensionless parameters: x_0 — layer thickness; x_λ — mean free path of carriers; y_0 — electric field frequency; g_1 and g_2 — parameters of surface roughness of the layer; and γ — ellipticity parameter that determines the degree of anisotropy of the constant energy surface. Parameters x_0, x_λ, g_1, and g_2 are normalized to de Broglie wavelength λ_{F0} of an electron with Fermi energy ε_{Fv}.

If the principal axis of the ellipsoid of revolution is codirectional with the Y axis, the longitudinal and transverse components of the conductivity tensor will swap places with each other. In the case of an arbitrary direction of the axis of rotation of the ellipsoid in plane (k_x, k_y), the expression for the conductivity tensor takes the form

$$\tilde{G} = \begin{pmatrix} G_\parallel \cos^2\varphi_0 + G_\perp \sin^2\varphi_0 & (G_\parallel - G_\perp)\cos\varphi_0 \sin\varphi_0 \\ (G_\parallel - G_\perp)\cos\varphi_0 \sin\varphi_0 & G_\parallel \sin^2\varphi_0 + G_\perp \cos^2\varphi_0 \end{pmatrix}, \quad (27)$$

where φ_0 is the angle between the principal axis of the ellipsoid of revolution and axis X.

3. Limit cases

Let us consider the case of a spherically symmetric energy band ($\gamma = 1$). The longitudinal and transverse components of the conductivity tensor are equal to each other:

$$\Sigma_{\parallel} = \Sigma_{\perp} = \frac{\gamma^2}{z_0}\left\{1 - \frac{3}{16x_0^3}\sum_{l=1}^{N}(\rho^2 - l^2)\chi\left(\frac{2x_0^2 z_0}{lx_\lambda}\right)\right\}, \tag{28}$$

$$z_0 = \frac{\rho}{2x_0} - iy_0.$$

Let us examine the limit transition to the quasi-classical case ($a \gg \lambda_B$, $a \lesssim \Lambda$). It follows from (19) and (20) that

$$N \approx \text{int}\,[\rho_v], \tag{29}$$

$$\rho^2 \approx \rho_v^2. \tag{30}$$

Since the energy spectrum of electrons is virtually continuous, one may switch from summation over subband number l to integration in expressions (25) and (26). The result is

$$\Sigma_{\parallel} = \frac{\gamma^2}{z_{0\parallel}}\left\{1 - \frac{3}{2}\int_0^1 (1-t^2)\chi\left(\frac{x_0 z_{0\parallel}\sqrt{\gamma}}{t}\right)dt\right\}, \tag{31}$$

$$\Sigma_{\perp} = \frac{1}{z_{0\perp}\gamma}\left\{1 - \frac{3}{2}\int_0^1 (1-t^2)\chi\left(\frac{x_0 z_{0\perp}\sqrt{\gamma}}{t}\right)dt\right\}. \tag{32}$$

The following notation was introduced here:

$$t = \frac{v_z}{v_{\text{F}\perp}}, \quad x_0 = \frac{a}{\Lambda},$$

where $v_{\text{F}\perp}$ is the Fermi velocity of an electron in the direction perpendicular to the axis of rotation of the Fermi ellipsoid. In the case of a degenerate electron gas, expressions (31) and (32) are consistent with the result reported in [29].

In the static case, the expressions for the longitudinal and transverse components of the conductivity tensor take the form corresponding to [18]:

$$\Sigma_{\parallel} = \frac{2x_0\gamma^{1.5}}{\rho}\left\{1 - \frac{3x_\lambda \rho}{32x_0^4\gamma^3}\sum_{l=1}^{N} l\left(1 - \frac{l^2}{\rho^2}\right)\chi\left(\frac{x_0\rho\gamma^{1.5}}{lx_\lambda}\right)\right\}, \tag{33}$$

$$\Sigma_{\perp} = \frac{2x_0}{\rho}\left\{1 - \frac{3x_\lambda \rho}{32x_0^4\gamma^{1.5}}\sum_{l=1}^{N} l\left(1 - \frac{l^2}{\rho^2}\right)\chi\left(\frac{x_0\rho}{lx_\lambda}\right)\right\}. \tag{34}$$

4. Analysis of the results

Figures 2 and 3 show the dependences of the modulus and argument of the dimensionless longitudinal component of the integral conductivity tensor on dimensionless thickness. Solid and dashed curves correspond to different values of ellipticity parameter γ. Oscillations with their period depending on the frequency of the electric field are seen. These oscillations may be attributed to the following factors. Since the perpendicular component of the wave vector is quantized at small nanolayer thicknesses, the projection of velocity onto the Z axis and the frequency of surface scattering of carriers will be discrete quantities. If period T of oscillations of the electric field strength is chosen in such a way that condition $\tau_s = nT$ is satisfied (τ_s is the time of propagation of a carrier from one boundary of the nanolayer to another and n is a positive integer), a

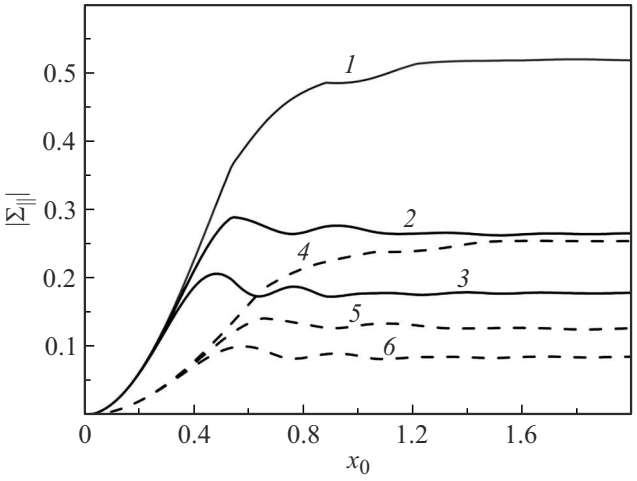

Figure 2. Dependences of the modulus of dimensionless longitudinal component $\Sigma_{\parallel}$ of the integral conductivity tensor on dimensionless thickness x_0 at $x_\lambda = 8$; $g_1 = g_2 = 0.2$, $\gamma = 2.32$ (solid curves *1–3*), $\gamma = 1.6$ (dashed curves *4–6*): *1* — $y_0 = 10$; *2* — $y_0 = 20$; *3* — $y_0 = 30$.

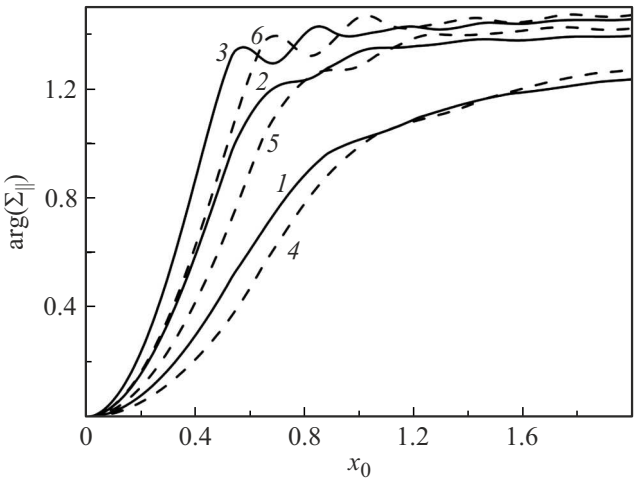

Figure 3. Dependences of the argument of dimensionless longitudinal component $\Sigma_{\parallel}$ of the integral conductivity tensor on dimensionless thickness x_0 at $x_\lambda = 8$; $g_1 = g_2 = 0.2$, $\gamma = 2.32$ (solid curves *1–3*), $\gamma = 1.6$ (dashed curves *4–6*): *1* — $y_0 = 10$; *2* — $y_0 = 20$; *3* — $y_0 = 30$.

certain fraction of carriers will be scattered by the surface of the nanolayer at the moment when the electric field strength vector changes its direction. When these carriers undergo surface scattering, the external electric field has no effect on them. Consequently, the distribution function of such carriers near the boundaries of the nanolayer will be equilibrium. It follows from boundary conditions (8) that the surfaces of the nanolayer will not affect the nature of motion of this group of carriers at $\tau_s = nT$. Owing to this, the modulus and argument of conductivity will be close to the case of a mirror surface at certain values of x_0 and y_0. Figure 3 demonstrates that the oscillation period decreases with increasing frequency, and the maxima shift to the left. At low frequencies, when $y_0 < 10$, oscillations of the modulus and phase of conductivity become weak. The Fermi surface anisotropy affects the oscillation period of the conductivity dependences on thickness: the oscillation period decreases with decreasing γ. This is attributable to a change in the ratio between the longitudinal and transverse effective masses of carriers that affect the surface scattering frequency. When γ decreases, the transverse effective mass of an electron grows smaller, while the surface scattering frequency increases (τ_s decreases). Note that the oscillation maxima of dashed curves are shifted toward larger x_0.

Figures 4 and 5 show the frequency dependences of the modulus and argument of the dimensionless longitudinal component of the conductivity tensor. It is evident that the conductivity modulus decreases with increasing frequency of the electric field. This is attributable to a delayed response of carriers at high frequencies, which makes their behavior similar to that of a set of bound charges that do not contribute to conductivity. Note that the frequency dependence of the conductivity modulus is monotonic and the conductivity phase oscillates with a change in frequency. The reason for the emergence of oscillations is similar

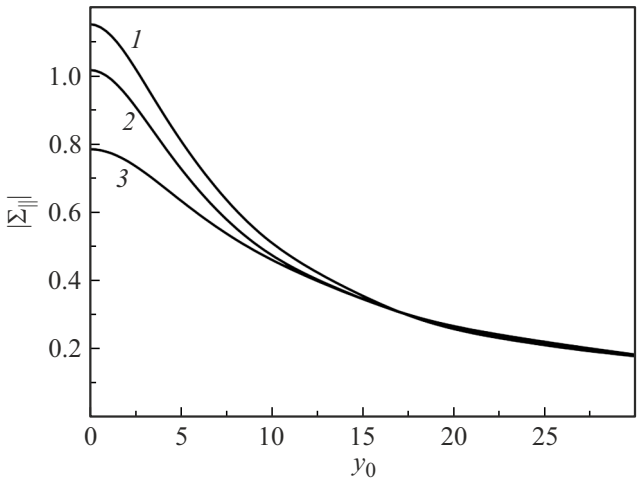

Figure 4. Dependences of the modulus of dimensionless longitudinal component $\Sigma_{||}$ of the integral conductivity tensor on dimensionless frequency y_0 at $x_0 = 0.8$ $x_\lambda = 8$; $\gamma = 2.32$; $g_2 = 0.15$: *1* — $g_1 = 0$; *2* — $g_1 = 0.06$; *3* — $g_1 = 0.15$.

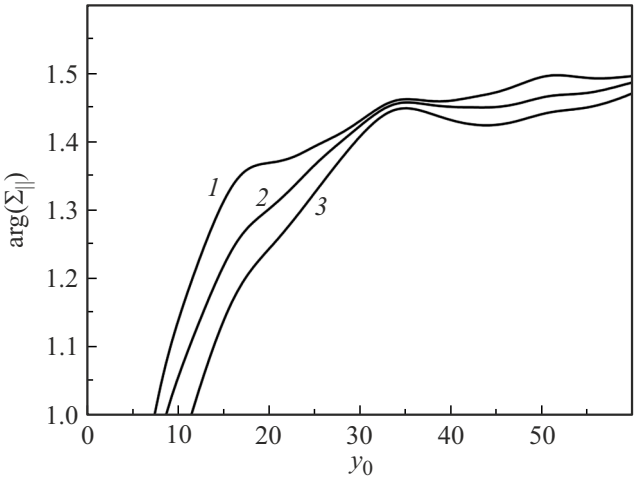

Figure 5. Dependences of the argument of dimensionless longitudinal component $\Sigma_{||}$ of the integral conductivity tensor on dimensionless frequency y_0 at $x_0 = 0.8$ $x_\lambda = 8$; $\gamma = 2.32$; $g_2 = 0.15$: *1* — $g_1 = 0$; *2* — $g_1 = 0.06$; *3* — $g_1 = 0.15$.

to the one detailed in the explanations to Figs. 2 and 3. With parameter y_0 being varied, condition $\tau_s = nT$ will be fulfilled periodically when the modulus and argument of conductivity are close to the case of specular scattering. The oscillation period in the case of identical roughness parameters of the upper and lower surfaces of the nanolayer (curve *3* in Fig. 5) is two times smaller than the oscillation period in the scenario where one surface of the nanolayer is mirror-like and the other is rough (curve *1* in Fig. 5). This is attributable to the fact that the frequency of surface scattering of carriers in the scenario characterized by curve *1* is two times lower than the scattering frequency corresponding to curve *3*. It is fair to say that the nature of carrier motion with one of the boundaries of the nanolayer being mirror-like is similar to that corresponding to a nanolayer of double the thickness with two rough boundaries. If the roughness parameters of the nanolayer boundaries are arbitrary (curve *2*), the frequency dependence of phase oscillates in a complex manner. Oscillations in this case take the form of a set of alternating more and less pronounced maxima of the conduction phase.

Figures 6 and 7 present the dependences of the modulus and argument of conductivity on ellipticity parameter γ of the Fermi surface. Solid curves follow the quantum theory of transport phenomena ((25) and (26)), while dashed curves were plotted in the quasi-classical approximation ((31) and (32)). The figures make it clear that the modulus and phase of the longitudinal component of the conductivity tensor decrease with increasing γ; in contrast, the modulus and phase of the transverse component increase. It can be seen from Figs. 6 and 7 that curves *1–4* converge at one point at $\gamma = 1$. This implies that the longitudinal and transverse components of conductivity are matching in a conductor with a spherical band structure. The dependences of the conductivity phase on the ellipticity parameter oscillate. The maximum difference between

the results obtained within the quantum and quasi-classical theories is observed in the case of the transverse direction of the principal axis of the Fermi ellipsoid. The quasi-classical approximation allows for an unlimited increase in conductivity modulus at $\gamma \ll 1$. This may be attributed to the small effective mass of carriers in the direction parallel to the electric field strength vector. Figure 1, *b* demonstrates that in the quantum case, a reduction in length of the secondary axis of the constant energy ellipsoid (a reduction in γ) translates into a lower carrier density due to a reduction in number of allowed energy states. As a result, the conductivity modulus cannot increase indefinitely at $\gamma \ll 1$.

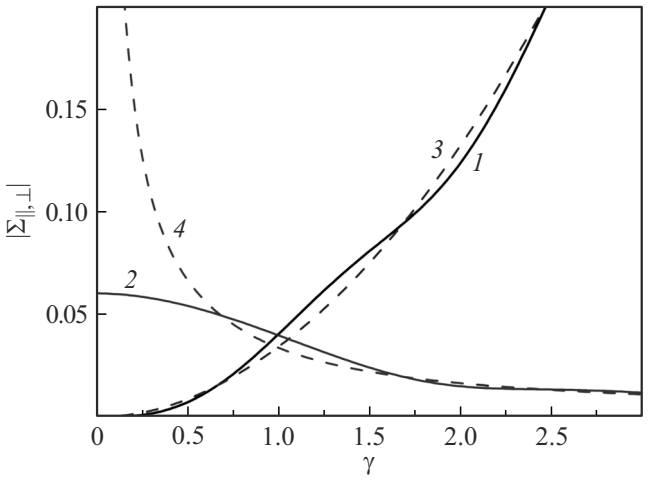

Figure 6. Dependences of the modulus of dimensionless longitudinal ($\Sigma_\parallel$, curves *1, 3*) and transverse ($\Sigma_\perp$, curves *2, 4*) components of the integral conductivity tensor on ellipticity parameter γ at $x_0 = 0.5$; $x_\lambda = 8$; $y_0 = 30$; $g_1 = 0$; $g_2 = 0.2$. Solid and dashed curves correspond to quantum and quasi-classical theories, respectively.

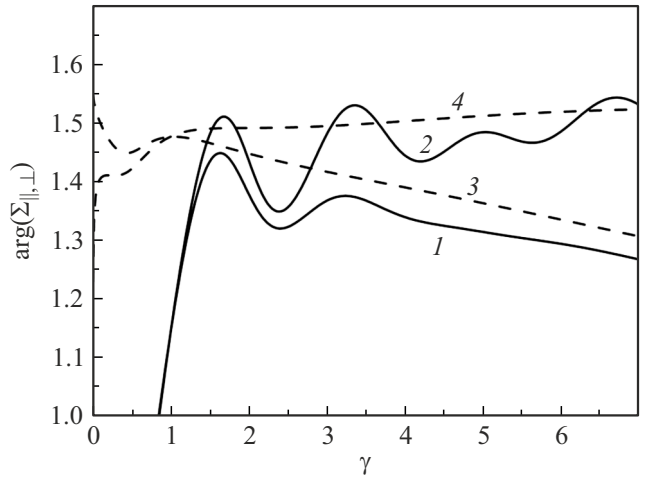

Figure 7. Dependences of the argument of dimensionless longitudinal ($\Sigma_\parallel$, curves *1, 3*) and transverse ($\Sigma_\perp$, curves *2, 4*) components of the integral conductivity tensor on ellipticity parameter γ at $x_0 = 0.5$; $x_\lambda = 8$; $y_0 = 30$; $g_1 = 0$; $g_2 = 0.2$. Solid and dashed curves correspond to quantum and quasi-classical theories, respectively.

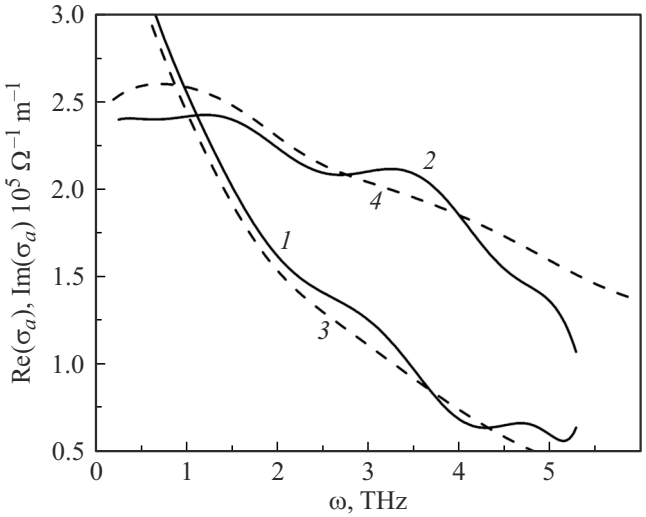

Figure 8. Frequency dependences of the real (curves *1, 3*) and imaginary (curves *2, 4*) parts of conductivity of a 70-nm-thick bismuth film. Solid curves *1, 2* represent the experimental data from [30]. Dashed curves *3, 4* are the result of theoretical calculations at $\lambda_{B0} = 27$ nm, $\Lambda = 1.8\,\mu$m; $\gamma = 0.4$; $g_1 = 0.1$; and $g_2 = 0.9$.

Figure 8 presents the dependences of the real and imaginary parts of conductivity of a bismuth film on the frequency of the electric field. Solid and dashed curves represent the experimental data from [30] and the result of theoretical calculations, respectively. Bismuth films were obtained by thermal evaporation at a temperature of 70 °C with subsequent annealing at 180 °C. These deposition conditions provided an opportunity to form bismuth films with a preferential orientation along trigonal axis C_3. This was confirmed by X-ray diffractometry and microphotographic images of the surface relief obtained using an atomic force microscope [30]. The authors of [30] found that the film consists of crystallites of a triangular shape. Neighboring crystallites are oriented relative to the common boundary in such a way that one of the crystallographic axes (binary C_1 or bisector C_2 one) does not change its direction, while the other axis is rotated by 180°. According to the authors of [30], the boundaries between grains with this orientation of crystallites in the sample have virtually no effect on conductivity. Surface scattering of carriers and quantum confinement remain the primary factors affecting the conductivity.

Orientation along the C_3 axis corresponds to the case where the principal axes of three ellipsoids of constant electron energy are virtually parallel to the film plane. The expression for conductivity averaged over the layer thickness, which is determined by the sum of conductivity components from electrons from each ellipsoid, was used to

compare theoretical calculations with experimental data:

$$\sigma_a = \frac{G}{a} = \frac{1}{a}\sum_{i=1}^{3} G_{xx}^{i} = \frac{1}{a}\sum_{i=1}^{3}\left\{ G_{\parallel}\cos^2\left(\chi + i\,\frac{2\pi}{3}\right) + G_{\perp}\sin^2\left(\chi + i\,\frac{2\pi}{3}\right)\right\} = \frac{3}{2a}\,(G_{\parallel} + G_{\perp}). \tag{35}$$

Here, χ is the angle between the principal axis of the Fermi ellipsoid and axis X. $G_{\parallel}$ and $G_{\perp}$ are specified by expressions (24)–(26).

Note that the conductivity of sufficiently thin bismuth films may behave similar to that of a semiconductor. This is attributable to a change in the relative position of energy bands within which the carriers are located. It was found in [31,32] that the critical thickness of a bismuth film corresponding to the emergence of semiconductor properties varies within the range of 25–30 nm. Experimental data for a bismuth film with a thickness of 70 nm were used for comparison with theoretical calculations. Bismuth is metallic in this case; i.e., one may use the theoretical model constructed here, which is applicable to metallic nanolayers, for comparison with the experiment.

The figures reveal close agreement between theoretical calculations and experimental data. The period of oscillations of solid curves matches the period of oscillations of the dashed ones. The difference lies in the position of oscillation maxima (minima) of conductivity. The observed differences in positions of oscillation maxima of the real and imaginary parts of conductivity are probably associated with the specific features of the band structure of bismuth and the presence of interellipsoidal transitions of carriers. The deviation between solid and dashed curves may be attributed to the fact that the Fermi energy was assumed here to vary with layer thickness, while the carrier density remained constant. It is likely that the thickness dependences of both parameters need to be taken into account in semi-metals, which will require a more detailed description of quantum transport phenomena.

Conclusion

Analytical expressions for the longitudinal and transverse components of the conductivity tensor of a metallic nanolayer as functions of the nanolayer thickness, the mean free path of carriers, the frequency of the electric field, the roughness parameters of nanolayer boundaries, and the ellipticity parameter of the Fermi surface were obtained with the effects of quantum confinement of carriers taken into account. Oscillations in the dependences of the modulus and phase of conductivity on thickness and frequency of the electric field were found. The amplitude of oscillations may be altered by varying the surface roughness parameters, while their position and period depend on frequency of the electric field. Oscillations in the frequency dependences of the modulus and phase of conductivity are well-pronounced in relatively thin nanolayers with a thickness comparable to the de Broglie wavelength of carriers at frequencies on the order of several tens of terahertz.

It was established that the anisotropy of the Fermi surface of a conductor affects the oscillation period of the dependences of the modulus and phase of conductivity on thickness. It was demonstrated that the conductivity modulus depends monotonically on the ellipticity parameter, while the corresponding dependence of the conductivity argument is oscillatory.

The veracity of the constructed theoretical model was confirmed via comparison of the obtained theoretical results with experimental data for a bismuth film. The observed differences in positions of oscillation maxima of the real and imaginary parts of conductivity are probably associated with the specific features of the band structure of bismuth, the presence of interellipsoidal transitions of carriers, etc.

Conflict of interest

The authors declare that they have no conflict of interest.

References

[1] S. Datta. *Quantum transport: Atom to Transistor* (Cambridge University Press, NY., 2005)

[2] C.P. Poole, F.J. Owens. *Introduction to Nanotechnology* (Wiley, 2003)

[3] V.Yu. Kireev. *Vvedenie v tekhnologii mikroelektroniki i nanotekhnologii* (Tsentr. Nauchno-Issled. Inst. Khim. Mekh., M., 2008) (in Russian)

[4] S.A. Yakovlev, I.Yu. Dmitriev, M.Yu. Mikhailov, K.V. Emtsev, A.S. Abramov, E.I. Terukov. Tech. Phys., **69** (10), 1580 (2024). DOI: 10.61011/JTF.2024.10.58865.173-24

[5] V.A. Nebol'sin, N. Swaikat, A.Yu. Vorob'ev, V.A. Yuryev. Tech. Phys. Lett., **49** (1), 75 (2023). DOI: 10.21883/TPL.2023.01.55355.19285

[6] A. Cavaleiro, J.Th.M. Hosson. *Nanostructured Coatings* (Springer, New York, 2006)

[7] K. Barmak, A. Darbal, K.J. Ganesh, P.J. Ferreira, J.M. Rickman, T. Sun, B. Yao, A.P. Warren, K.R. Coffey. J. Vac. Sci. Tech. A, **32**, 061503 (2014). DOI: 10.1116/1.4894453

[8] L. Moraga, K.F. Arenas, R. Henriquez, S. Bravo, B. Solis. Physica B: Condens. Matt., **499**, 17 (2016). DOI: 10.1016/j.physb.2016.07.001

[9] T. Zhou, D. Gall. Phys. Rev. B, **97**, 165406 (2018). DOI: 10.1103/PhysRevB.97.165406

[10] R.L. Graham, G.B. Alers, T. Mountsier, N. Shamma, S. Dhuey, S. Cabrini, R.H. Geiss, D.T. Read, S. Peddeti. Appl. Phys. Lett., **96**, 042116 (2010). DOI: 10.1063/1.3292022

[11] A.A. Pribylov. J. Vac. Sci. Tech. B, **39**, 022804 (2021). DOI: 10.1116/6.0000781

[12] I.A. Kuznetsova, O.V. Savenko, A.A. Yushkanov. Tech. Phys., **62** (12), 1766 (2017). DOI: 10.1134/S1063784217120143

[13] P.A. Kuznetsov, O.V. Savenko, A.A. Yushkanov. Tech. Phys., **65** (12), 1912 (2020). DOI: 10.1134/S1063784220120130

[14] L. Sheng, D.Y. Xing, Z.D. Wang. Phys. Rev. B, **51**, 7325 (1995). DOI: 10.1103/PhysRevB.51.7325

[15] R.C. Munoz, C. Arenas. Appl. Phys. Rev., **4**, 011102 (2017). DOI: 10.1063/1.4974032
[16] A.E. Meyerovich, A. Stepaniants. J. Phys.: Condens. Matter, **12**, 5575 (2000). DOI: 10.1088/0953-8984/12/26/305
[17] S. Chatterjee, A.E. Meyerovich. Phys. Rev. B, **84**, 165432 (2011). DOI: 10.1103/PhysRevB.84.165432
[18] I.A. Kuznetsova, O.V. Savenko, D.N. Romanov. Phys. Lett. A, **427**, 127933 (2022). DOI: 10.1016/j.physleta.2022.127933
[19] S.B. Soffer. J. Appl. Phys., **38** (4), 1710 (1967).
[20] O.V. Savenko, I.A. Kuznetsova. Proc. SPIE, **12157**, 121570W (2022). DOI: 10.1117/12.2622544
[21] B.A. Tavger, V.Ya. Demikhovskiĭ. Sov. Phys. Usp., **11**, 644 (1969). DOI: 10.1070/PU1969v011n05ABEH003739
[22] V.S. Édel'man. Sov. Phys. Usp., **20**, 819 (1977). DOI: 10.1070/PU1977v020n10ABEH005467
[23] E.V. Demidov, V.M. Grabov, V.A. Komarov, A.N. Krushelnitckii, A.V. Suslov, M.V. Suslov. Semiconductors, **53** (6), 727 (2019). DOI: 10.1134/S1063782619060046
[24] G.A. Ivanov, V.M. Grabov. Fiz. Tekh. Poluprovodn., **29** (5), 1040 (1995) (in Russian).
[25] L.A. Fal'kovskiĭ. Sov. Phys. Usp, **11** (1), 1 (1968). DOI: 10.1070/PU1968v011n01ABEH003 721
[26] M.V. Suslov, V.M. Grabov, V.A. Komarov, E.V. Demidov, S.V. Senkevich, A.V. Suslov. Semiconductors, **53**, 589 (2019). DOI: 10.1134/S1063782619050257
[27] K. Blum. *Density Matrix Theory and Applications* (Springer, 1981)
[28] V.P. Kurbatsky, V.V. Pogosov. Phys. Rev. B, **81**, 155404 (2010). DOI: 10.1103/PhysRevB.81.155404
[29] O.V. Savenko, P.A. Kuznetsov, I.A. Kuznetsova. J. Phys.: Conf. Series. **1697**, 012094 (2020). DOI: 10.1088/1742-6596/1697/1/012094
[30] A. Zaitsev, P. Demchenko, E. Makarova, A. Tukmakova, N. Kablukova, A. Asach, A. Novotelnova, M. Khodzitsky. Phys. Stat. Sol. RRL. **14**, 2000093 (2020). DOI: 10.1002/pssr.202000093
[31] C.A. Hoffman, J.R. Meyer, F.J. Bartoli. Phys. Rev. B, **48** (15), 11431 (1993). DOI: 10.1103/PhysRevB.48.11431
[32] D.E. Martínez-Lara, R. González-Campuzano, D. Mendoza. Thin Solid Films, **821**, 140678 (2025). DOI: 10.1016/ j.tsf.2025.140678

Translated by D.Safin

Appendix

Derivation of the kinetic equation

Within perturbation theory, Hamiltonian $\hat{H}$ may be presented as

$$\hat{H}(t) = \hat{H}_0 + \hat{V}(t), \tag{A1}$$

where $\hat{H}_0$ is the eigen-Hamiltonian of an electron and $\hat{V}$ is the time-dependent potential of transition between eigenstates.

With (A1) taken into account, the equation for matrix elements of density operator $\rho_{l'l}$ then takes the form [27]

$$i\hbar \frac{\partial \rho_{l'l}}{\partial t} = (\varepsilon_{l'} - \varepsilon_l)\rho_{l'l} + \sum_{l_1}(V_{l'l_1}\rho_{l_1l} - \rho_{l'l_1}V_{l_1l}). \tag{A2}$$

Here, ε_l is the eigenvalue of Hamiltonian $\hat{H}_0$ and $V_{l'l_1}$ is the matrix element of operator $\hat{V}$.

The equation for diagonal elements of the density matrix (distribution function) $f_l = \rho_{ll}$ is written as follows:

$$\frac{\partial f_l}{\partial t} = -\frac{i}{\hbar}\sum_{l_1}(V_{ll_1}\rho_{l_1l} - \rho_{ll_1}V_{l_1l}). \tag{A3}$$

In the non-stationary case, Eq. (A3) may be rewritten as

$$\frac{\partial f_l}{\partial t} = \left(\frac{\partial f_l}{\partial t}\right)_F - \frac{i}{\hbar}\sum_{l_1}(V_{ll_1}\rho_{l_1l} - \rho_{ll_1}V_{l_1l}). \tag{A4}$$

The first term on the right-hand side of the equation characterizes the change in distribution function f_l under the influence of an external electric field. The second term characterizes the distribution function variation induced by scattering of carriers.

An expression for the first term of Eq. (A4) was obtained in [18], where a constant electric field was considered:

$$\left(\frac{\partial f_l}{\partial t}\right)_F = \frac{\hbar k_{zl}}{m_\perp}\frac{\partial f_l}{\partial z} + \frac{e\mathbf{E}}{\hbar}\frac{\partial f_l}{\partial k_\parallel}, \tag{A5}$$

where $k_{zl} = \pi l/a$ is the transverse component of the wave vector of an electron in the lth subband and $\mathbf{k}_\parallel$ is the component of the wave vector of a carrier parallel to the nanolayer plane.

The second term of Eq. (A4) is associated with the probability of carrier transition W_{l_1l} from state l to state l_1 as a result of volume scattering [18]:

$$\frac{\partial f_l}{\partial t} = -\sum_{l_1} W_{l_1l}(f_l - f_{l_1}), \tag{A6}$$

$$W_{l_1l} = \frac{2\pi}{\hbar}|V^0_{ll_1}|^2\delta(\varepsilon_{l_1} - \varepsilon_l),$$

where $V^0_{ll_1}$ is the matrix element of the potential of carrier scattering off one impurity.

In the case of an ellipsoidal band structure of a metal, the right-hand side of Eq. (A6) may be expressed in terms of components of the relaxation time tensor. Let us consider this issue in detail. Taking into account the expansion of function f_l (7) that is linear in the external field, the collision integral may be rewritten as

$$\frac{\partial f_l}{\partial t} = -\sum_{l_1} W_{l_1l}(f^{(1)}_l - f^{(1)}_{l_1}). \tag{A7}$$

We assume that the carrier scattering is elastic. Let us switch to a coordinate system in the space of wave vectors such that the Fermi surface has spherical symmetry:

$$\begin{cases} \tilde{k}_x = \sqrt{m_0/m_\parallel}k_x, \\ \tilde{k}_y = \sqrt{m_0/m_\perp}k_y, \\ \tilde{k}_{zl} = \sqrt{m_0/m_\perp}k_{zl}. \end{cases} \tag{A8}$$

The expression for the total energy in this coordinate system takes the form

$$\varepsilon_l = \frac{\hbar^2 \tilde{k}_x^2}{2m_0} + \frac{\hbar^2 \tilde{k}_y^2}{2m_0} + \frac{\hbar^2 \tilde{k}_{zl}^2}{2m_0}. \tag{A9}$$

Non-equilibrium corrections to the distribution function $f_l^{(1))}$ and $f_{l_1}^{(1)}$, which were obtained through expansion linear in the external field, may be presented as the sum of products of functions depending on the carrier energy by the components of the longitudinal wave vector $\tilde{\mathbf{k}}_\parallel$:

$$f_l^{(1)}(z, \tilde{\mathbf{k}}_\parallel) = f_{l\parallel}^{(1)}(z, \tilde{\mathbf{k}}_\parallel) + f_{l\perp}^{(1)}(z, \tilde{\mathbf{k}}_\parallel) = \chi_\parallel(\varepsilon_l)\tilde{k}_x + \chi_\perp(\varepsilon_l)\tilde{k}_y, \tag{A10}$$

$$f_{l_1}^{(1)}(z, \tilde{\mathbf{k}}_\parallel) = f_{l_1\parallel}^{(1)}(z, \tilde{\mathbf{k}}_\parallel) + f_{l_1\perp}^{(1)}(z, \tilde{\mathbf{k}}_\parallel) = \chi_\parallel(\varepsilon_{l_1})\tilde{k}_x + \chi_\perp(\varepsilon_{l_1})\tilde{k}_y. \tag{A11}$$

Inserting (A10) and (A11) into (A7), we obtain an expression for the volume collision integral:

$$\frac{\partial f_l}{\partial t} = -\chi_\parallel(\varepsilon_l)\tilde{k}_x \sum_{l_1} W_{l_1 l}\left(1 - \frac{\chi_\parallel(\varepsilon_{l_1})}{\chi_\parallel(\varepsilon_l)}\right) - \chi_\perp(\varepsilon_l)\tilde{k}_y \sum_{l_1} W_{l_1 l}\left(1 - \frac{\chi_\perp(\varepsilon_{l_1})}{\chi_\perp(\varepsilon_l)}\right). \tag{A12}$$

Note that the resulting factor in brackets depends only on the energy of carriers in the lth and l_1th subbands. In the $(\tilde{k}_x, \tilde{k}_y, \tilde{k}_z)$ coordinate system, the transition matrix in the case of elastic carrier scattering depends only on the modulus of the wave vector (energy of carriers). We may then introduce the carrier relaxation time

$$\sum_{l_1} W_{l_1 l}\left(1 - \frac{\chi_\perp(\varepsilon_{l_1})}{\chi_\perp(\varepsilon_l)}\right) = \frac{1}{\tau} \tag{A13}$$

and rewrite expression (A12) in the form

$$\frac{\partial f_l}{\partial t} = -\frac{\chi_\parallel(\varepsilon_l)\tilde{k}_x}{\tau} - \frac{\chi_\perp(\varepsilon_l)\tilde{k}_y}{\tau}. \tag{A14}$$

Switching to the old coordinates in the space of wave vectors, we obtain

$$\frac{\partial f_l}{\partial t} = -\frac{\chi_\parallel(\varepsilon_l)}{\tau}\sqrt{\frac{m_\parallel}{m_0}}\,k_x - \frac{\chi_\perp(\varepsilon_l)}{\tau}\sqrt{\frac{m_\perp}{m_0}}\,k_y = \frac{f_{l\parallel}^{(1)}}{\tau_\parallel} + \frac{f_{l\perp}^{(1)}}{\tau_\perp}, \tag{A15}$$

where $\tau_\parallel$ and $\tau_\perp$ are the longitudinal and transverse components of the relaxation time tensor.

Thus, the kinetic equation takes the form

$$-i\omega\left(f_{l\parallel}^{(1)} + f_{l\perp}^{(1)}\right) + \frac{\hbar k_{zl}}{m_\perp}\frac{\partial\left(f_{l\parallel}^{(1)} + f_{l\perp}^{(1)}\right)}{\partial z} + \frac{e\mathbf{E}}{\hbar}\frac{\partial f_l^{(0)}}{\partial \mathbf{k}_\parallel} + \frac{f_{l\parallel}^{(1)}}{\tau_\parallel} + \frac{f_{l\perp}^{(1)}}{\tau_\perp} = 0. \tag{A16}$$